

Article

Local Heat Transfer Dynamics in the In-Line Tube Bundle under Asymmetrical Pulsating Flow

Aigul Haibullina ^{1,*}, Aidar Khairullin ^{1,*}, Denis Balzamov ¹, Vladimir Ilyin ¹, Veronika Bronskaya ^{2,3} and Liliya Khairullina ³

¹ Institute of Heart Power Engineering, Kazan State Power Engineering University, 51 Krasnoselskaya Street, 420066 Kazan, Russia

² Mechanical Faculty, Kazan National Research Technological University, 68 Karl Marx Street, 420015 Kazan, Russia

³ Engineering Institute of Computer Mathematics and Information Technologies, Kazan Federal University, 18 Kremlyovskaya Street, 420008 Kazan, Russia

* Correspondence: haybullina.87@mail.ru (A.H.); kharullin@yandex.ru (A.K.)

Abstract: The pulsating flow is one of the techniques that can enhance heat transfer, therefore leading to energy saving in tubular heat exchangers. This paper investigated the heat transfer and flow characteristics in a two-dimensional in-line tube bundle with the pulsating flow by a numerical method using the Ansys Fluent. Numerical simulation was performed for the Reynolds number $Re = 500$ with different frequencies and amplitude of pulsation. Heat transfer enhancement was estimated from the central tube of the tube bundle. Pulsation velocity had an asymmetrical character with a reciprocating flow. The technique developed by the authors to obtain asymmetric pulsations was used. This technique allows simulating an asymmetric flow in heat exchangers equipped with a pulsation generation system. Increase in both the amplitude and the frequency of the pulsations had a significant effect on the heat transfer enhancement. Heat transfer enhancement is mainly observed in the front and back of the cylinder. At a steady flow in these areas, heat transfer is minimal due to the weak circulation of the flow. The increase in heat transfer in the front and back of the cylinder is associated with increased velocity and additional flow mixing in these areas. The maximum increase in the Nusselt number averaged over space and time in the entire studied range was 106%, at a pulsation frequency of 0.5 Hz and pulsation amplitude of 4.5. A minimum enhancement of 25% was observed at a frequency of 0.166 Hz and amplitude of 1.25.

Keywords: asymmetric pulsating flow; in-line tube bundle; CFD; enhancement of heat transfer



Citation: Haibullina, A.; Khairullin, A.; Balzamov, D.; Ilyin, V.; Bronskaya, V.; Khairullina, L. Local Heat Transfer Dynamics in the In-Line Tube Bundle under Asymmetrical Pulsating Flow. *Energies* **2022**, *15*, 5571. <https://doi.org/10.3390/en15155571>

Academic Editors: Nazrul Islam, Dibakar Rakshit, Saleem Anwar Khan, Abdullatif A. Gari, Abdus Samad and Amjad Ali Pasha

Received: 29 June 2022

Accepted: 29 July 2022

Published: 31 July 2022

Publisher's Note: MDPI stays neutral with regard to jurisdictional claims in published maps and institutional affiliations.



Copyright: © 2022 by the authors. Licensee MDPI, Basel, Switzerland. This article is an open access article distributed under the terms and conditions of the Creative Commons Attribution (CC BY) license (<https://creativecommons.org/licenses/by/> 4.0).

1. Introduction

Cross-flow tube bundles are widely used in various heat exchange equipment. Shell and tube heat exchangers are commonly used in the power, food, chemical, and petrochemical industries. Therefore, improving the efficiency of such equipment can lead to significant energy savings. Improving the efficiency of shell-and-tube heat exchangers is closely related to heat transfer enhancement techniques. The use of various techniques for heat exchange augmentation can lead to a decrease in the metal consumption of heat exchange equipment, a reduction in the capacities required for pumping, and a decrease in the consumption of heat carriers. The accumulated literature in this area includes thousands of references and continues to grow [1–5].

Both passive and active techniques are used to heat transfer enhancement. Passive methods include twisted tube bundles [6], tubes with spiral grooves [7], tubes with spiral finning [8], tube bundles with different diameters [9], etc. The active method includes the application of an electromagnetic field [10], vibration [11], or rotation [12] of the heat exchange surface, etc.

Artificially created pulsation of the fluid flow is one of the active heat transfer enhancement techniques. Many authors [13–16] have studied pulsating flows to enhance heat transfer. Kikuchi et al. [17] studied the heat transfer of a single cylinder in a pulsating flow numerically and experimentally. The work in [17] showed that increasing the frequency and amplitude of pulsations leads to heat transfer enhancement. The increase in heat transfer occurs at the front and back of the cylinder. The maximum values of the instantaneous Nusselt number were observed at pulsation phases corresponding to the maximum flow velocity. Fu et al. and Zheng et al. [18,19] investigated the heat transfer of a single cylinder in a pulsating flow numerically. The authors in [18] concluded that the heat transfer increased due to the synchronization of the natural frequency of the vortex shedding in the wake of the cylinder and the forced frequency of pulsations (the phenomenon of vortex resonance or lock-on) [20]. Heat transfer enhancement was mainly observed in the back of the cylinder, while in [19], it was at the front of the cylinder. Heat transfer increases with an increase in the pulsating frequency. The lock-on occurs when the forced frequency of pulsations is twice the natural frequencies from the natural shedding vortices in a steady flow. The enhancement of heat transfer has a maximum value in lock-on regime. The increase in heat transfer occurs due to vortices being shed at the same frequency as the forced pulsating frequency. A further increase in the ratio of the pulsation frequency and natural frequencies leads to a decrease in heat transfer intensification. The authors in [17–19] noted that the maximum instantaneous values of the Nusselt number were observed at pulsation phases corresponding to the maximum flow velocities. The heat transfer of a single square cylinder in the pulsating flow was experimentally investigated by Ji et al. [20]. The maximum enhancement of heat transfer was observed when the pulsation frequencies were twice as high as the natural frequencies of the vortex oscillations. In [21], the effect of an oscillating cylinder on heat transfer was investigated numerically. It was shown that heat transfer increased with increasing amplitude and frequency of pulsations. The field synergy principle was applied to study the heat transfer enhancement mechanisms. It was found that streamlines become disordered behind the cylinder with increasing amplitude. With increasing frequency, the intensity of the vortices behind the cylinder increased. The authors in [22,23] analyzed the formation of vortex structures in the wake of a single cylinder in a pulsating airflow. A relationship between vortex structures with heat exchange was established. It was shown that the maximum heat transfer augmentation was observed at the back of the cylinder, which corresponded to the flow regime with the formation of two symmetric vortices in the cylinder wake. The authors associated the increase in heat transfer with the disturbing flow structure at the back of the cylinder. The authors determined [24,25] the flow and heat transfer characteristics of in-line and staggered tube bundles at symmetric air pulsations. Flow pulsations lead to an increase in heat transfer due to the disturbing vortex flow structures in the annular space of the tube bundles. For the in-line tube bundle, the maximum increase in heat transfer was 42%, while for the staggered tube bundle it was 16%. Liang et al. [26] studied pulsating sinusoidal flows in an in-line tube bundle numerically using the large eddy simulation (LES) technique. An increase in heat transfer from the cylinder of the first and second rows was obtained, which was associated with the phenomenon of vortex resonance. Wu et al. [27] experimentally investigated the external heat exchange of a staggered tube bundle immersed in water. In this study, the situation of a heat exchanger immersed in seawater was simulated. It was found that an increase in the amplitude was practically proportional to an increase in the heat transfer of the tube bundle. A change in the wave frequency had almost no effect on the heat transfer augmentation. The authors in [28] numerically investigated heat transfer at symmetric pulsations in a staggered tube bundle. It was shown that heat transfer augmentation changed with the pulsation regime and the row of the tube bundle. Mulcahey et al. [29] investigated the heat transfer of a ten-row tandem of square tubes with symmetric flow pulsations. The results are presented for different tube spacing. It can be seen that the heat transfer depends on the geometry and flow regimes.

Hydrodynamics and heat transfer in a transverse flow around tube bundles in a steady flow has been well-studied [30–33]. However, there are very few similar studies with pulsating flows. Most of the work has been devoted to a single cylinder. In the case of pulsating flows, at least two more are added to the similarity criteria used in a steady flow: the Strouhal number and the amplitude of the pulsations, which complicates the study, even for a single cylinder. The problem is more complicated for bundles of tubes by the sheer number of configurations encountered in practice. In the works related to the research topic, the pulsations are symmetrical and the mechanisms of heat transfer augmentation have not been fully revealed [34]. Many researchers have concluded that the intensification of heat transfer in pulsating flows is associated with the phenomenon of vortex resonance [20,35–37]. Additionally, authors [17,19,22,24,38,39] have mentioned the restructuring of the flow structure, a decrease in the boundary layer, the mixing of large-scale vortex structures, and additional turbulization of the flow.

This work investigates the mechanisms leading to heat transfer enhancement in the in-line tube bundle with asymmetric flow pulsations. Numerical simulations are presented for the Strouhal numbers St 0.038, 0.057, 0.114; amplitude A/D 1.25, 3, 4.5; and Reynolds number Re 500.

2. Mathematical Model

2.1. Computational Domain and Boundary Conditions

The computational domain of the model is a bundle of tubes (Figure 1) that is bounded on all sides by halves of tubes. The diameter of the tubes is $D = 0.01$. The relative transverse and longitudinal pitch are $s_{1,2}/D = 1.3$. The 2D in-line tube bundle was employed to simplify the mathematical model. Satisfactory agreement with the experimental data with a 2D formulation was obtained in [28,40,41] for systems similar to the flow field studied in this work. A constant temperature $t_w = 42$ and a no slip condition ($U_x = 0, U_y = 0$) were set on all walls of the tubes. A constant flow temperature $t_f = 27$ was set to the computational domain at the inlet, and a symmetry condition ($\partial U_x / \partial n = 0, \partial U_y / \partial n = 0, \partial p / \partial n = 0$) on the top and bottom of the domain. At the outlet, constant pressure $P = 101,325$. Water was chosen as the working fluid. The thermophysical properties of water were calculated depending on the flow temperature.

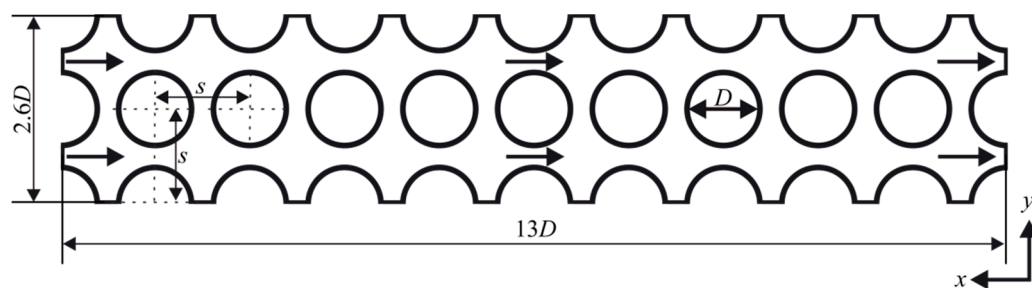


Figure 1. The computational domain.

For a steady flow at the inlet to the computational domain, a constant flow velocity u was set corresponding to the Reynolds number $Re = 500$. The Reynolds numbers were calculated as follows:

$$Re = Du/\eta,$$

where η is the kinematic viscosity of water. The pulsating asymmetric flow at the inlet of the computational domain was set according to Figure 2. The asymmetric flow corresponded to the required frequency f and the dimensionless relative amplitude A/D of the pulsations, where A is the dimensional amplitude found by the equation:

$$A = \langle u_p \rangle \tau,$$

where $\langle u_p \rangle$ is the pulsation flow velocity averaged over time τ for the corresponding negative values of instantaneous pulsation velocity u_p :

$$\langle u_p \rangle = \frac{\int_{\tau_1}^{\tau_2} u_p d\tau}{\tau_2 - \tau_1},$$

where τ_1 is the start time of the pulsation period; τ_2 is the end time of the pulsation period.

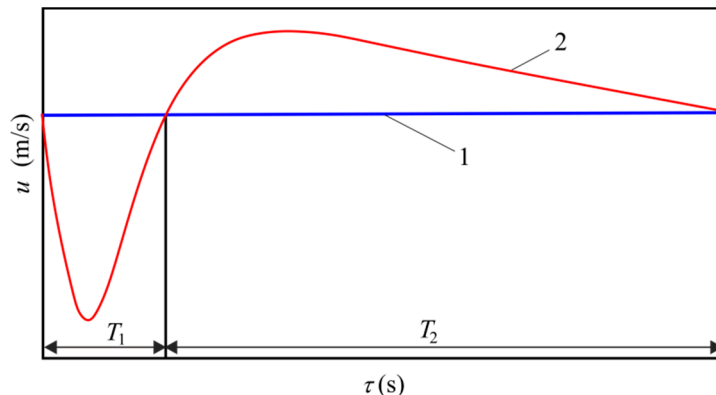


Figure 2. Pulsating asymmetric flow: 1—steady flow; 2—pulsating velocity.

The pulsating frequency is found by equation:

$$f = 1/T,$$

where T is the pulsation period consisting of two half periods:

$$T = T_1 + T_2,$$

where T_1 is the first pulsation half-period; T_2 is the second half-period. The steady flow velocity u_{st} is equal to the pulsation flow velocity $\langle u_p \rangle$ averaged over the pulsation period:

$$u_{st} = \langle u_p \rangle = \frac{\int_0^T u_p d\tau}{T}.$$

The Strouhal number is defined as:

$$St = fD/u.$$

The pulsation velocity has an asymmetrical character with a reciprocating flow. The technique developed by the authors to obtain asymmetric pulsations was used. This technique simulates an asymmetric flow in heat exchangers equipped with a pulsation generation system [42]. Figure 3 shows a scheme of the hydraulic model for generating a pulsating flow with a reciprocating flow in a tube bundle. The geometric parameters of the system elements for generating pulsation flows in the tube bundle corresponded to the experimental setup parameters [42].

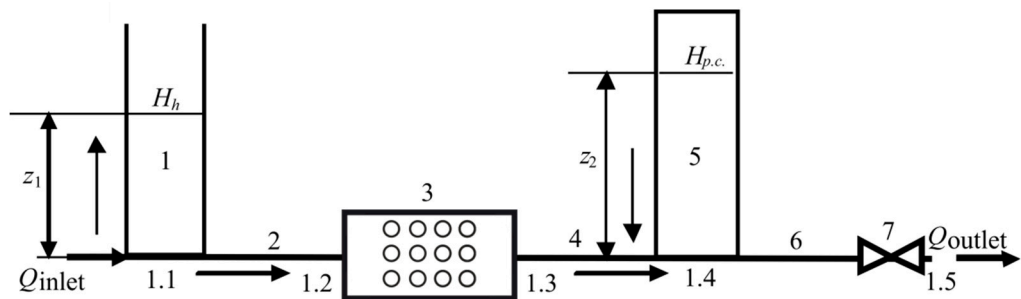


Figure 3. A scheme of the hydraulic model to generate a pulsating flow: 1—hydraulic accumulator, 2, 4, 6—pipes, 3—tube bundle, 5—pulsation chamber, 7—valve.

To find the change in flow rates and pressure over time, a system of differential-algebraic Equations (1)–(8) was solved. The flow rate at nodes 1.1–1.5 can be defined by equations:

$$Q_{\text{inlet}} - Q_1 - Q_2 = 0, \quad (1)$$

$$Q_4 - Q_5 - Q_6 = 0, \quad (2)$$

where Q_{inlet} , Q_1 , Q_2 , Q_4 , Q_5 , Q_6 are the volumetric flow rate of hydraulic model elements according to Figure 3. The flow rate in hydraulic accumulator 1 is defined by the relation:

$$\frac{dQ_1}{d\tau} = gS_1 \frac{H_1 - (H_h + z_1)}{z_1} - \left[\frac{k_1}{2D_{j1}S_1} + \left(\frac{S_1}{S_{h0}} \right)^2 \right] Q_1 |Q_1|, \quad (3)$$

$$\frac{dz_1}{d\tau} = \frac{Q_1}{S_1}, \quad (4)$$

where H_1 and H_h are pressure in node 1.1 and on the surface of the liquid in the hydraulic accumulator 1, respectively. S_{h0} is the connecting hole area with node 1.1 at the bottom of the hydraulic accumulator. D_{j1} , k_1 , and S_1 are the diameter, area, and hydraulic resistance coefficient in the hydraulic accumulator 1, respectively. g is the gravity acceleration. z_1 is the liquid level in the hydraulic accumulator.

The flow rate in pipes 2, 4, and tube bundle 3 is defined by the relation:

$$\left(\frac{l_2}{S_2} + \frac{l_3}{S_3} + \frac{l_4}{S_4} \right) \frac{dQ_2}{d\tau} = gS_2(H_1 - H_4) - Q_2 |Q_2| \left(\frac{k_2 l_2}{2D_{j2} S_2} + \frac{k_3 l_3}{2D_{j3} S_3} + \frac{k_4 l_4}{2D_{j4} S_4} \right), \quad (5)$$

where l_2 , l_3 , l_4 are the length of the hydraulic model elements according to Figure 3. k_2 , k_3 , k_4 are the hydraulic resistance coefficient of the hydraulic model elements according to Figure 3. S_2 , S_3 , S_4 are the area of the hydraulic model elements according to Figure 3. D_{j2} , D_{j3} , D_{j4} are the diameter of the hydraulic model elements according to Figure 3. H_4 is the pressure in node 1.4.

The flow rate in pulsation chamber 5 was carried out by the following relations:

$$\frac{dQ_5}{d\tau} = gS_5 \frac{H_4 - z_2 - H_{p.c.}}{z_2} - \left[\frac{k_5}{2D_{j5}S_5} + \left(\frac{S_5}{S_{p.c.0}} \right)^2 \right] Q_5 |Q_5|, \quad (6)$$

$$\frac{dz_2}{d\tau} = \frac{Q_5}{S_5}, \quad (7)$$

where $S_{p.c.0}$ is the connecting hole area with node 1.5 at the bottom of the pulsation chamber. H_4 is the pressure on the surface of the liquid in pulsation chamber 5. z_2 is the liquid level in the pulsation chamber.

The flow rate in pipe 6 is defined by the relation:

$$\frac{l_6}{S_6} \frac{dQ_6}{d\tau} = g(H_4 - H_h) - Q_6 |Q_6| \left(k_6 \frac{l_6}{D_{j6} S_6^2} + k_7 \frac{1}{S_7^2} \right) \quad (8)$$

where l_6 is the length of pipe 6. k_6, k_7 are the hydraulic resistance coefficient of pipe 6 and valve 7. S_6 is the area of pipe 6. D_{j6} is the diameter of the hydraulic model elements according to Figure 3.

The coefficient of hydraulic resistance k was found according to the empirical formulas [43]. The required flow rate was set at the inlet of the hydraulic model. The pressure dependence on time $H_{p.c.}(t)$ was set to generate a pulsating flow in the pulsating chamber. The shape of the $H_{p.c.}(t)$ dependence was obtained on an experimental setup in [42]. The system of Equations (1)–(8) was solved by Newton's iterative method [43].

In Figure 4, the results obtained by solving Equations (1)–(8) are compared with the experimental data [42]. The obtained results are in good agreement with the experimental data; the deviation from the calculated data was 2%.

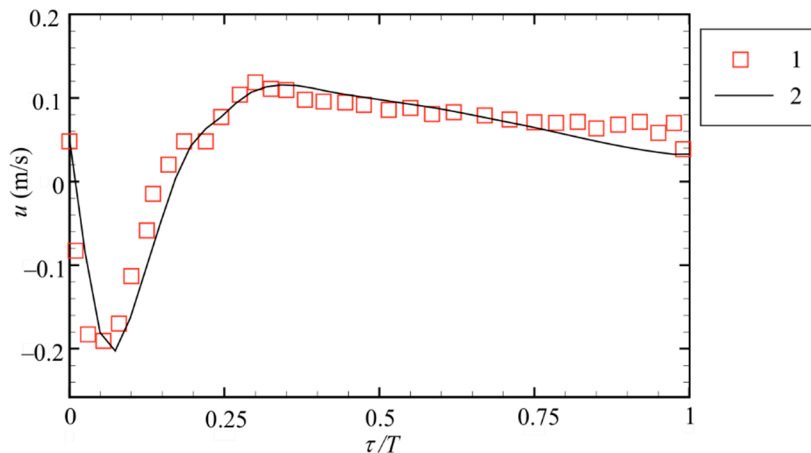


Figure 4. The pulsating velocity at $f = 0.5$ Hz, $A/D = 3$, $Re = 500$: 1—experimental data [42]; 2—numerical simulation.

2.2. Modeling Approach

The flow of an incompressible fluid was calculated by the Reynolds averaged Navier–Stokes equation. The simple one-equation model Spalart–Allmaras (SA) [44] was used as a turbulence model, which requires a lower computational cost. Wang et al. [45] showed that the SA model in a two-dimensional setting could predict the flow characteristics in a tube bundle. The maximum mesh size related to the tube diameter was $y_{max}/D = 0.2$. The minimum cell size in the near-wall region is $r_{min}/D = 3.16 \times 10^{-2}$. The grid size in the near-wall region expanded in the radial direction with a factor of 1.2. The number of layers in the near-wall region was 10. The convergence of a grid solver with similar systems to this work was carried out by Kim et al. and Mulcahey et al. [29,46]. In the present study, the maximum mesh size was 0.2 mm. In works [29,46], a sufficient element size was 0.2 mm and higher. The mesh of the computational domain is shown in Figure 5. Mathematical modeling was carried out in Ansys Fluent, with a coupled solution algorithm based on the pressure-based solver. For all calculations, the SIMPLE algorithm was used. Except for the energy equation, the residual was less than 10^{-4} for all of the governing equations. A convergence criterion of 10^{-6} was used for the energy equation for the residuals. The time step was 0.01 s. For time stepping, the first order implicit transient formulation was used.

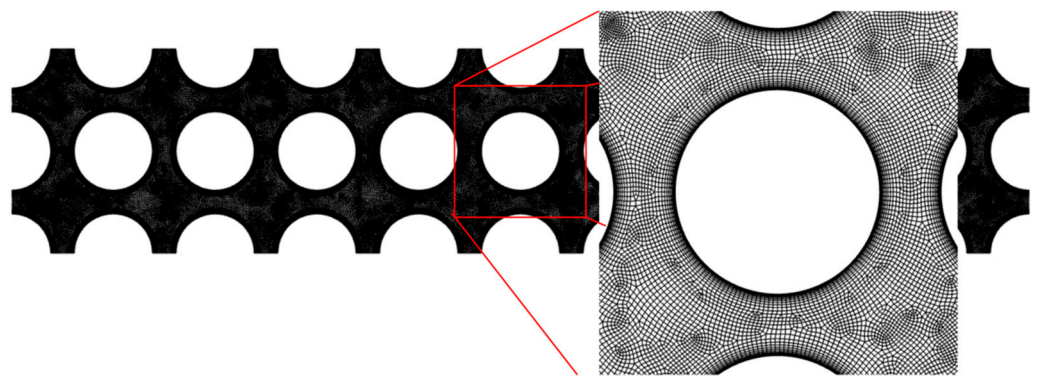


Figure 5. The mesh of the computational domain.

2.3. Methodology for Evaluating Results of Simulation

The flow and heat transfer characteristics used in the analysis of the obtained results were calculated for the central cylinder in the fifth row of the tube bundle. The heat flux q averaged over the surface of the wall q_o was found by Equation (9) over the surface, and over time $\langle q_o \rangle$ using Equation (10). The local heat flux q_ϕ averaged depending on the azimuth angle— φ (Figure 6) by Equation (11), and q_ϕ averaged over time by Equation (12).

$$q_o = \frac{\int_0^{360} q d\phi}{\pi D}, \quad (9)$$

$$\langle q_o \rangle = \frac{\int_0^T q_o d\tau}{T}, \quad (10)$$

$$q_\phi = \frac{\int_{\phi_1}^{\phi_2} q d\phi}{\pi D/8}, \quad (11)$$

$$\langle q_\phi \rangle = \frac{\int_0^T q_\phi d\tau}{T}. \quad (12)$$

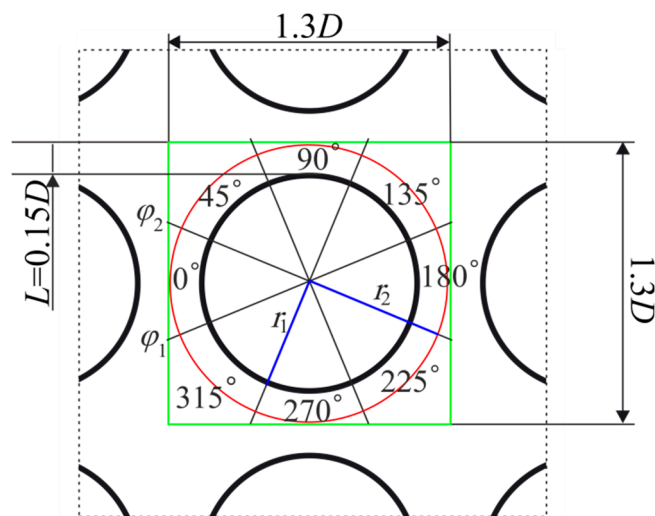


Figure 6. The location of the azimuth angle and the annular region around the cylinder of the fifth row of the tube bundle to determine the flow characteristics and heat transfer.

The temperature of water t_s was averaged over the area around the cylinder for $x = [x_1; x_2] = [0; 1.3D]$ $y = [y_1; y_2] = [0; 1.3D]$ (Figure 6) and was found by Equation (13). The temperature averaged over space and time $\langle t_s \rangle$ was found by Equation (14).

$$t_s = \frac{\int_{y_1}^{y_2} \int_{x_1}^{x_2} t dx dy}{(1.3D)^2 - \pi D^2 / 4}, \quad (13)$$

$$\langle t_s \rangle = \frac{\int_0^T t_s d\tau}{T}. \quad (14)$$

The velocity U was found according to Equation (15). The velocity U_a averaged over the sector area around the cylinder with the thickness $L = 0.15D$ (Figure 6) was found according to Equation (16), and over space and time $\langle U_a \rangle$ according to Equation (17). The local fluid velocity U_ϕ is averaged depending on the azimuth angle ϕ according to Equation (18), and U_ϕ is time-averaged $\langle U_\phi \rangle$ according to Equation (19).

$$U = |U| = \sqrt{U_x^2 + U_y^2}, \quad (15)$$

where $U_{x,y}$, is the velocity component.

$$U_a = \frac{\int_{r_1}^{r_2} \int_0^{360} U d\phi dr}{F(\phi, r)}, \quad (16)$$

where $F(\phi, r)$ is the area of the sector around the cylinder.

$$\langle U_a \rangle = \frac{\int_0^T U_a d\tau}{T}, \quad (17)$$

$$U_\phi = \frac{\int_{r_1}^{r_2} \int_{\phi_1}^{\phi_2} U d\phi dr}{F(\phi, r)}, \quad (18)$$

$$\langle U_\phi \rangle = \frac{\int_0^T U_\phi d\tau}{T}. \quad (19)$$

The effective thermal conductivity λ_{eff} averaged over the annular region around the cylinder $\lambda_{eff,a}$ was determined by Equation (20), and over space and time $\langle \lambda_{eff,a} \rangle$ by Equation (21). The local effective thermal conductivity $\lambda_{eff,\phi}$ and local effective thermal conductivity averaged over time $\langle \lambda_{eff,\phi} \rangle$ were found according to Equations (22) and (23), respectively.

$$\lambda_{eff,a} = \lambda_a + \lambda_{turb,a}, \quad (20)$$

$$\langle \lambda_{eff,a} \rangle = \langle \lambda_a \rangle + \langle \lambda_{turb,a} \rangle, \quad (21)$$

$$\lambda_{eff,\phi} = \lambda_\phi + \lambda_{turb,\phi}, \quad (22)$$

$$\langle \lambda_{eff,\phi} \rangle = \langle \lambda_\phi \rangle + \langle \lambda_{turb,\phi} \rangle, \quad (23)$$

where λ , λ_{turb} are the thermal and turbulent thermal conductivity of the water. λ , λ_{turb} in Equations (20)–(23) was defined similarly to Equations (16)–(19).

The temperature difference Δt was found according to Equation (24), averaged over time $\langle \Delta t \rangle$ according to Equation (25).

$$\Delta t = t_{wall} - t_s, \quad (24)$$

$$\langle \Delta t \rangle = t_{wall} - \langle t_s \rangle. \quad (25)$$

The Nusselt number averaged over space Nu_o was found according to Equation (26), and over space and time $\langle Nu_o \rangle$ according to Equations (26) and (27). The local Nusselt number averaged over one-eighth of the region around the cylinder Nu_ϕ and over time $\langle Nu_\phi \rangle$ were determined by Equations (28) and (29).

$$Nu_o = \frac{q_0 D}{\Delta t \lambda_a}, \quad (26)$$

$$\langle Nu_o \rangle = \frac{\int_0^T Nu_o d\tau}{T}, \quad (27)$$

$$Nu_\phi = \frac{q_\phi D}{\Delta t \lambda_\phi}, \quad (28)$$

$$\langle Nu_\phi \rangle = \frac{\int_0^T Nu_\phi d\tau}{T}. \quad (29)$$

2.4. Model Verification

In [47], a comparative evaluation of the applicability of various RANS models to model heat transfer in an in-line tube bundle at a steady flow was carried out. SA, shear stress transport (SST), and Reynolds stress model (RSM) were compared through empirical correlation [32]. The models showed good agreement with the empirical correlation. The difference in heat transfer at a Reynolds number of 500 for the SA, SST, and RSM models with the empirical correlation was 12.6%, 14.6%, and 11.5%, respectively. The SA model was chosen to simulate the pulsating flow by taking into account its computational cost. Figure 7 shows the results of the numerical simulation and experimental data [42] for the pulsating flow at the Reynolds number of 500. According to Figure 7, the numerical simulation results are in agreement with the experimental data. The experimental and numerical simulation difference averaged 17%, with an experimental data error of 12%.

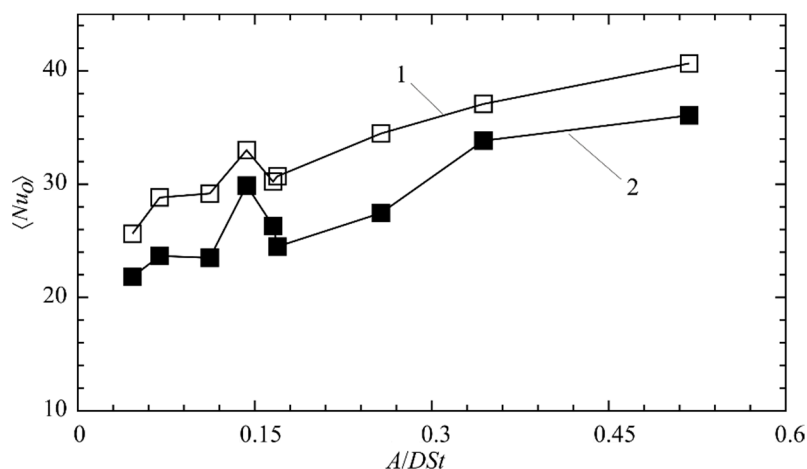


Figure 7. Variation of $\langle Nu_o \rangle$ with A/DSt : 1—experimental data [42]; 2—numerical simulation.

3. Results and Discussion

Simulations were performed for the Prandtl number $Pr = 6.2$, and the Reynolds number $Re = 500$, which allowed us to validate the model with the experimental data [42]. In this work, pulsations with reciprocating motion were studied. Therefore, the amplitude of pulsations A/D was 1.25, 3, and 4.5. Due to the large amplitudes of pulsations, low-frequency pulsations were used in this work. The pulsation frequency f is 0.166 Hz, 0.25 Hz, and 0.5 Hz, which corresponds to the Strouhal numbers St 0.038, 0.057, and 0.114, respectively. The relative transverse and longitudinal pitch was s/D 1.3. Tube bundles with a pitch of 1.3 are widely used in tubular heat exchangers.

3.1. Effect of Amplitude and Frequency of Pulsations on the Flow and Heat Transfer Characteristics

Figure 8 shows the effect of the amplitude A/D and the pulsation frequency f on the augmentation in the velocity $\langle \delta U_a \rangle = \langle U_{a,p} \rangle / U_{a,st}$, heat flux $\langle \delta q_o \rangle = \langle q_{o,p} \rangle / q_{o,st}$, Nusselt number $\langle \delta Nu_o \rangle = \langle Nu_{o,p} \rangle / Nu_{o,st}$, temperature difference $\langle \delta \Delta t \rangle = \langle \Delta t_p \rangle / \Delta t_{st}$, and effective thermal conductivity $\langle \delta \lambda_{eff,a} \rangle = \langle \lambda_{eff,a,p} \rangle / \lambda_{eff,a,st}$. The averaged over space and time velocity, heat flux, Nusselt number, and effective thermal conductivity were higher with higher amplitude. The temperature difference was almost the same (change less than 0.2%). The augmentation of heat transfer with an increase in the amplitude of pulsations correlated with the increase in the flow velocity and the effective thermal conductivity. The temperature difference stayed the same (change less than 0.3%) with increased pulsation frequency, while an increase in the heat flux and velocity was observed. The increase in the effective thermal conductivity was no more than 0.5%. The maximum augmentation of the averaged over space and time velocity, heat flux, and effective thermal conductivity was 3.18, 2.32, 1.4 times, respectively, at $A/D = 4.5, f = 0.5$ Hz. The maximum increase in the Nusselt number averaged over space and time across the entire studied range was 106% at $f = 0.5$ Hz ($St = 0.114$), $A/D = 4.5$, the minimum was 25% at $f = 0.166$ Hz ($St = 0.038$), and $A/D = 1.25$, which is consistent with the data from other authors. In [24], with symmetric pulsations in the in-line tube bundle, an augmentation of 42% was obtained at $St = 0.3$. The Strouhal number was higher than in our study. However, the amplitude of the velocity pulsations was 0.42 without reciprocating flow. In [27], at higher amplitudes of $A/D = 18.5$, a heat transfer augmentation of 200% was achieved. In [26], by a pulsating flow at $St = 0.45$, the enhancement of heat transfer occurred only at the front of the second cylinder in the tube bundle. Other cylinders in the tube bundle were not much affected by the external pulsation. The lack of heat transfer enhancement was associated with a low pulsation amplitude without reciprocating flow. The velocity pulsation amplitude was 0.1. In [29], the heat transfer enhancement ratio in the tube bundles increased with the pulsation frequency, which also agreed with the data presented in this study.

The maximum enhancement of the averaged Nusselt number over space and time $\langle \delta Nu_o \rangle$ was observed at the maximum frequency and amplitude of pulsations. The minimum augmentation of the Nusselt number $\langle \delta Nu_o \rangle$ corresponded to the minimum frequency and amplitude of pulsations. In the studied range, an increase in frequency had a greater effect on the heat transfer enhancement in comparison with the amplitude of pulsations. For example, at a fixed frequency $f = 0.25$ Hz with an increase in the amplitude A/D from 1.25 to 4.5, the augmentation of the Nusselt number averaged over space and time at $A/D = 1.25$ was 1.35 and 1.57 times at $A/D = 4.5$. With an increase in the frequency f from 0.166 Hz to 0.5 Hz at a fixed amplitude $A/D = 3$, the Nusselt number averaged over space and time at $f = 0.166$ Hz was 1.35 and 1.94 times at $f = 0.5$ Hz.

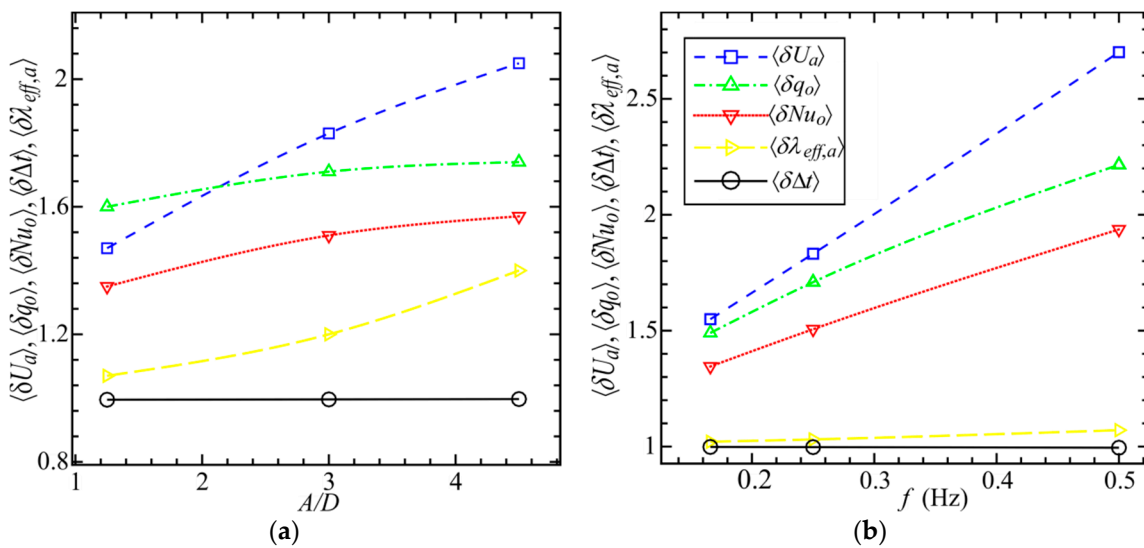


Figure 8. The effect of the pulsations on the flow and heat transfer characteristics averaged over space and time. **(a)** Variation of the velocity ratio $\langle \delta U_a \rangle = \langle U_{a,p} \rangle / U_{a,st}$, heat flux ratio $\langle \delta q_o \rangle = \langle q_{o,p} \rangle / q_{o,st}$, Nusselt number ratio $\langle \delta Nu_o \rangle = \langle Nu_{o,p} \rangle / Nu_{o,st}$, temperature difference ratio $\langle \delta \Delta t \rangle = \langle \Delta t_p \rangle / \Delta t_{st}$, and effective thermal conductivity ratio $\langle \delta \lambda_{eff,a} \rangle = \langle \lambda_{eff,a,p} \rangle / \lambda_{eff,a,st}$ with A/D at $f = 0.25$ Hz. **(b)** Variation of $\langle \delta U_a \rangle$, $\langle \delta q_o \rangle$, $\langle \delta Nu_o \rangle$, $\langle \delta \Delta t \rangle$, $\langle \delta \lambda_{eff,a} \rangle$ with f at $A/D = 3$.

Figure 9 shows the dynamics of δU_a , δq_o , δNu_o , $\delta \Delta t$, and $\delta \lambda_{eff,a}$ for one period of pulsations at a frequency $f = 0.5$ Hz. The increase in instantaneous values of the flow velocity δU_a , heat flux δq_o , and the effective thermal conductivity $\delta \lambda_{eff,a}$ averaged over the area around the cylinder was higher, so the higher the pulsation amplitude. The instantaneous values of the heat flux and effective thermal conductivity at $A/D = 4.5$ during the period of pulsations increased up to 3.57 and 2.23 times compared to the steady flow, respectively. The instantaneous values of the flow velocity increased up to 9.5 times for a separate pulsation phase, while by the end of the pulsation period at $\tau/T > 0.8$, the instantaneous flow velocity was less than the steady flow. The maximum instantaneous augmentation temperature difference $\delta \Delta t = 1.31$ was observed at the minimum pulsation amplitude, which is the opposite to δU_a , δq_o , δNu_o , and $\delta \lambda_{eff,a}$. The averaged instantaneous values of the Nusselt number δNu_o increased up to 3.37 times at amplitude $A/D = 4.5$ and a pulsation phase $\tau/T = 0.3$. A slight decrease in the Nusselt number δNu_o up to 0.9 times, in a pulsating flow compared to a steady flow, was observed at an amplitude $A/D = 1.25$ and a pulsation phase $\tau/T = 0.3$. When considering the dynamics of instantaneous values of increases in the effective thermal conductivity and the Nusselt number over time, two peaks were observed (Figure 9b,e). The first peak was observed up to $\tau/T = 0.25$, which corresponded to the first half-period of pulsations T_1 ; the second peak was observed after $\tau/T = 0.25$, which corresponded to the second half-period of pulsations T_2 . The fluid flow in the tube bundle was characterized by a reciprocating flow. Therefore, the first maximum of the values δNu_o and $\delta \lambda_{eff,a}$, was associated with the acceleration of the fluid flow during its flow in the opposite direction (Figure 4). The second maximum was related to the acceleration of the fluid flow during its flow in the forward direction (second half-period of pulsations T_2). For instantaneous values of heat flux and velocity (Figure 9a,c) there was one significant peak during T_1 and a second less noticeable one during T_2 . Both peaks were also associated with the accelerations of the fluid flow from pulsation. The more significant value of the first velocity peak (Figure 9c) was associated with the asymmetric nature of the flow pulsations at the inlet to the computational domain. The maximum velocity amplitude values at the tube bundle inlet were higher at the first half-period of pulsation than the second half-period of pulsation. The velocity amplitude values were the difference between the steady flow velocity and instantaneous pulsating velocity. Differences between the velocity amplitude values were higher with higher pulsation amplitude A/D . At the

minimum value of the pulsation amplitudes $A/D = 1.25$, the velocity values of the peaks were close (Figure 9c). Obviously, with decreasing pulsation amplitude, the peak of the first half-period of pulsation will become smaller than the peak of the second half-period of pulsation.

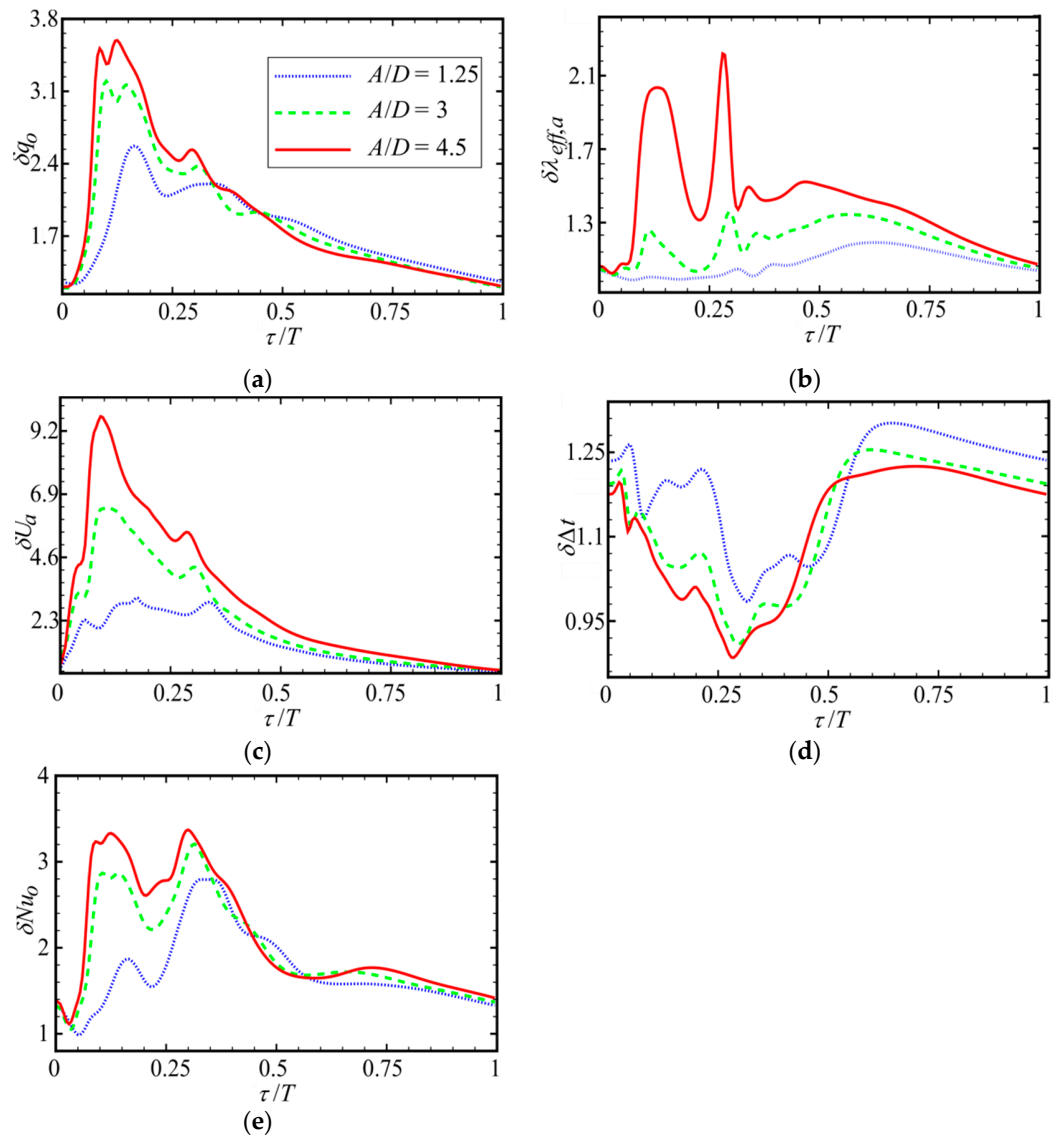


Figure 9. The effect of pulsations on instantaneous flow and heat transfer characteristics averaged over space at $f = 0.5$ Hz for one period of pulsation. (a) Variation of heat flux ratio $\delta q_0 = q_{0,p}/q_{0,st}$ with τ/T . (b) Variation of effective thermal conductivity ratio $\delta \lambda_{eff,a} = \lambda_{eff,a,p}/\lambda_{eff,a,st}$ with τ/T . (c) Variation of velocity ratio $\delta U_a = U_{a,p}/U_{a,st}$ with τ/T . (d) Variation of temperature difference ratio $\delta \Delta t = \Delta t_p/\Delta t_{st}$ with τ/T . (e) Variation of Nusselt number ratio $\delta Nu_0 = Nu_{0,p}/Nu_{0,st}$ with τ/T .

A decrease in the instantaneous values of the temperature difference $\delta \Delta t$ during the first half-period of pulsations was caused by the reversal flow. The increase in heat transfer with the increase in the instantaneous velocity at the asymmetric pulsation correlates with the data of other authors [17–19], where the pulsations were symmetric.

3.2. Effect of Amplitude and Frequency of Pulsations on Local Flow Characteristics and Heat Transfer

Figures 10–12 shows the variation in the local values of the heat flux $\langle \delta q_\varphi \rangle$, the effective thermal conductivity $\langle \delta \lambda_{eff,\varphi} \rangle$, the velocity $\langle \delta U_\varphi \rangle$, and the Nusselt number $\langle \delta Nu_\varphi \rangle$ with the amplitude A/D and the frequency f of pulsations. Increasing the pulsation frequency

had a greater effect on the Nusselt number averaged over one-eighth of the cylinder area $\langle \delta Nu_{\varphi} \rangle$ compared to increasing the pulsation amplitude. The local Nusselt number $\langle \delta Nu_{\varphi} \rangle$, in a pulsating flow compared to a steady flow at $\varphi = 0^\circ$ and 180° , increased from 4 to 9.5 times with increasing frequency (Figure 12b). As the amplitude increased, the Nusselt number $\langle \delta Nu_{\varphi} \rangle$ at $\varphi = 0^\circ$ and 180° increased from 4 to 5.5 times (Figure 12a). The minimum enhancement of the local Nusselt number $\langle \delta Nu_{\varphi} \rangle$ was observed at $\varphi = 90^\circ$, at $A/D = 3$, $f = 0.166$ Hz $\langle \delta Nu_{\varphi} \rangle = 1.04$. When $f = 0.25$ Hz and $A/D = 3$ for $\varphi = 90^\circ$, there was a decrease in the local value of the Nusselt number by 1%. The maximum increase in velocity $\langle \delta U_{\varphi} \rangle$ in a pulsating flow with an increase in the amplitude and frequency of pulsations (Figures 10c and 11c) was observed at $\varphi = 0^\circ$ and 180° , which is consistent with the increase in the local heat flux (Figures 10a and 11a) and the Nusselt number (Figure 12). In the A/D range from 3 to 4.5, a slight decline in the growth $\langle \delta U_{\varphi} \rangle$ was observed for $\varphi = 0^\circ$ and 180° (Figure 10c), while the values of $\langle \delta q_{\varphi} \rangle$, $\langle \delta Nu_{\varphi} \rangle$ also declined at $\varphi = 180^\circ$ and decreased at $\varphi = 0^\circ$ (Figures 10a and 12a). The maximum growth of the effective thermal conductivity $\langle \delta \lambda_{eff,\varphi} \rangle$, with increasing A/D and f was observed at $\varphi = 45^\circ$ (Figures 10b and 11b), and the minimum at $\varphi = 0^\circ$ and 180° , which was the opposite to $\langle \delta q_{\varphi} \rangle$, $\langle \delta Nu_{\varphi} \rangle$, $\langle \delta U_{\varphi} \rangle$. The maximum absolute values of $\langle \delta q_{\varphi} \rangle$, $\langle \delta Nu_{\varphi} \rangle$, $\langle \delta U_{\varphi} \rangle$ were observed at $\varphi = 0^\circ$ and 180° , and the minimum at $\varphi = 45^\circ$ and 90° .

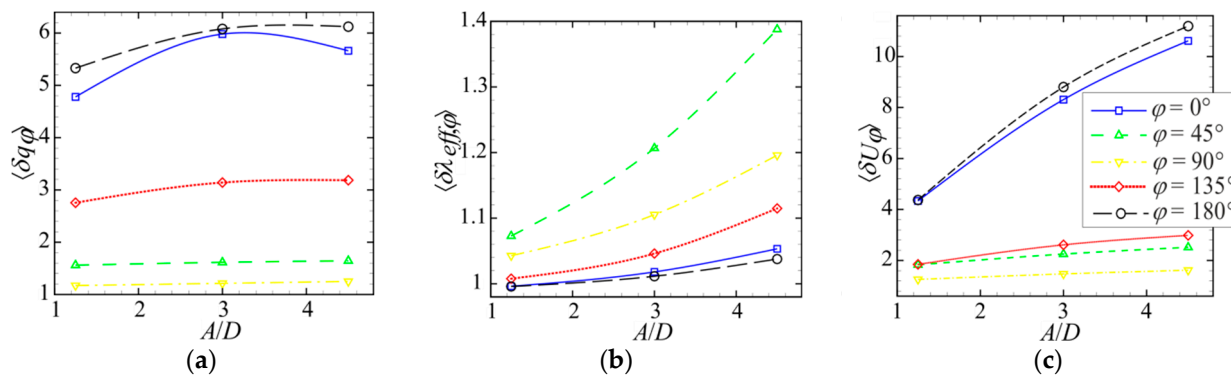


Figure 10. The effect of pulsations on the local flow and heat transfer characteristics at $f = 0.25$ Hz. (a) Variation of heat flux ratio $\langle \delta q_{\varphi} \rangle = \langle q_{\varphi,p} \rangle / q_{\varphi,st}$ with A/D . (b) Variation of effective thermal conductivity ratio $\langle \delta \lambda_{eff,\varphi} \rangle = \langle \lambda_{eff,\varphi,p} \rangle / \lambda_{eff,\varphi,st}$ with A/D . (c) Variation of velocity ratio $\langle \delta U_{\varphi} \rangle = \langle U_{\varphi,p} \rangle / U_{\varphi,st}$ with A/D .

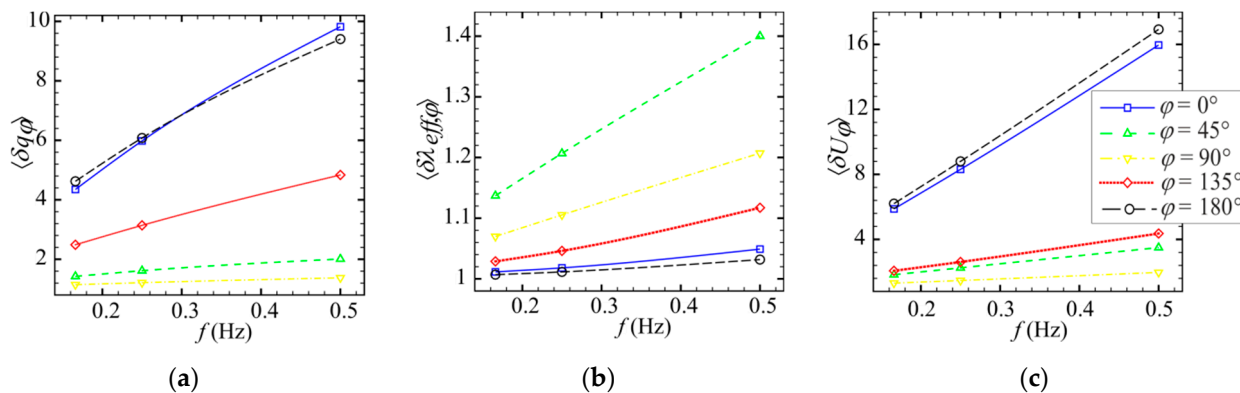


Figure 11. The effect of pulsations on the local flow and heat transfer characteristics at $A/D = 3$. (a) Variation of $\langle \delta q_{\varphi} \rangle = \langle q_{\varphi,p} \rangle / q_{\varphi,st}$ with f . (b) Variation in the effective thermal conductivity ratio $\langle \delta \lambda_{eff,\varphi} \rangle = \langle \lambda_{eff,\varphi,p} \rangle / \lambda_{eff,\varphi,st}$ with f . (c) Variation in the velocity ratio $\langle \delta U_{\varphi} \rangle = \langle U_{\varphi,p} \rangle / U_{\varphi,st}$ with f . The effect of pulsations on the local flow and heat transfer characteristics at $A/D = 3$. (a) The variation in the heat flux ratio $\langle \delta q_{\varphi} \rangle = \langle q_{\varphi,p} \rangle / q_{\varphi,st}$ with f . (b) Variation in the effective thermal conductivity ratio $\langle \delta \lambda_{eff,\varphi} \rangle = \langle \lambda_{eff,\varphi,p} \rangle / \lambda_{eff,\varphi,st}$ with f . (c) Variation in the velocity ratio $\langle \delta U_{\varphi} \rangle = \langle U_{\varphi,p} \rangle / U_{\varphi,st}$ with f .

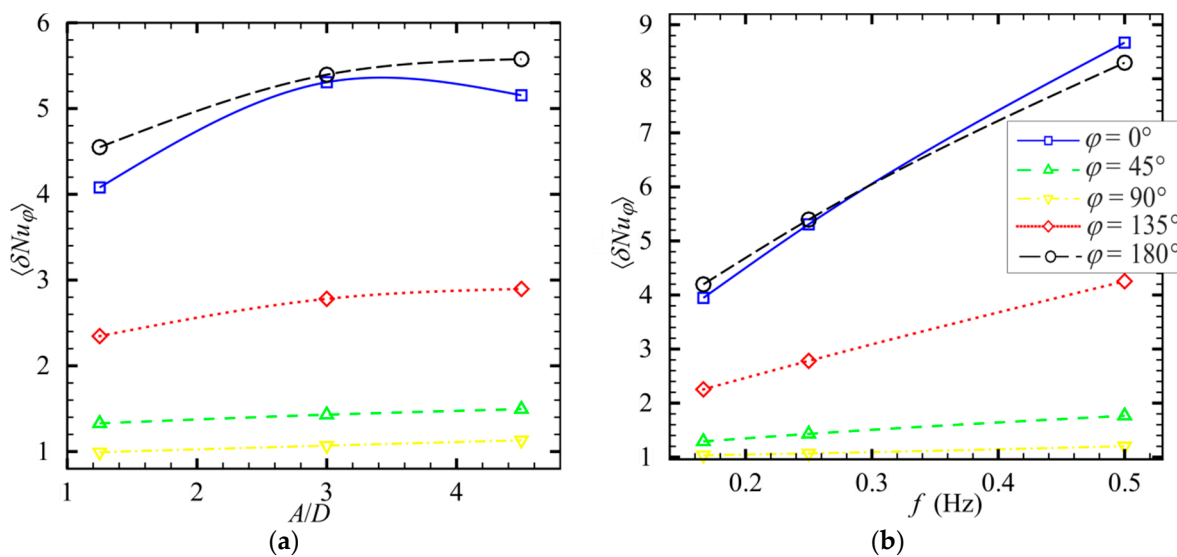


Figure 12. The effect of pulsations on the local Nusselt number. (a) Variation in the Nusselt number ratio $\langle \delta Nu_\varphi \rangle = \langle Nu_{\varphi,p} \rangle / Nu_{\varphi,st}$ with A/D at $f = 0.25$ Hz. (b) Variation of $\langle \delta Nu_\varphi \rangle = \langle Nu_{\varphi,p} \rangle / Nu_{\varphi,st}$ with f at $A/D = 3$.

In the in-line tube bundles with a steady flow between the rows of the tube, regions with low circulation are formed. As a result, the heat transfer in these areas is reduced [32,33]. An increase in the intensity of pulsations leads to an increase in the fluid circulation in these areas (Figures 10c and 11c). Therefore, with an increase in the intensity of the pulsations, an increase in heat transfer occurs in the front ($\varphi = 0^\circ$) and back ($\varphi = 180^\circ$) areas of the cylinder.

The local dynamics of the instantaneous values of δU_φ , δq_φ , δNu_φ , $\delta \lambda_{eff,\varphi}$ are shown in Figures 13 and 14. The values of local heat flux δq_φ and local Nusselt number δNu_φ in the front ($\varphi = 0^\circ$) and back part ($\varphi = 135^\circ$, 180°) of the cylinder increased up to 14–29 times, which is consistent with an increase in the values of δU_φ . The instantaneous value of the local Nusselt number at the front of the cylinder ($\varphi = 0^\circ$) increased up to 29 times (Figure 14d) during the first pulsation period T_1 , which corresponded to the reciprocating flow. The augmentation of the instantaneous values of the local Nusselt number in the front part of the cylinder was associated with the restructuring of the flow structure, as the result of the reciprocating flow. The maximum augmentation of δNu_φ in the back of the cylinder ($\varphi = 180^\circ$) reached 16 times. The maximum augmentation at ($\varphi = 180^\circ$) was observed during the second period of pulsations T_2 , which corresponded to the flow acceleration, which led to heat transfer intensification.

For the instantaneous local effective thermal conductivity $\delta \lambda_{eff,\varphi}$ a rise to 1.4 was observed at $\varphi = 45^\circ$, $A/D = 1.25$ (Figure 14a) during the second half-period T_2 , while the instantaneous local Nusselt number δNu_φ at $\varphi = 45^\circ$ did not increase (Figure 14c). Consequently, an increase in $\delta \lambda_{eff,\varphi}$ to 1.4 is insufficient for heat transfer augmentation. It can be assumed that the heat transfer enhancement at $A/D = 1.25$ was mainly associated with the increase in the flow velocity. When $A/D = 4.5$, the instantaneous effective thermal conductivity $\delta \lambda_{eff,\varphi}$ increased up to 3.5 times at $\varphi = 45^\circ$, 90° , and 135° (Figure 14b), which is consistent with the growth of δq_φ and δNu_φ for this region of the cylinder.

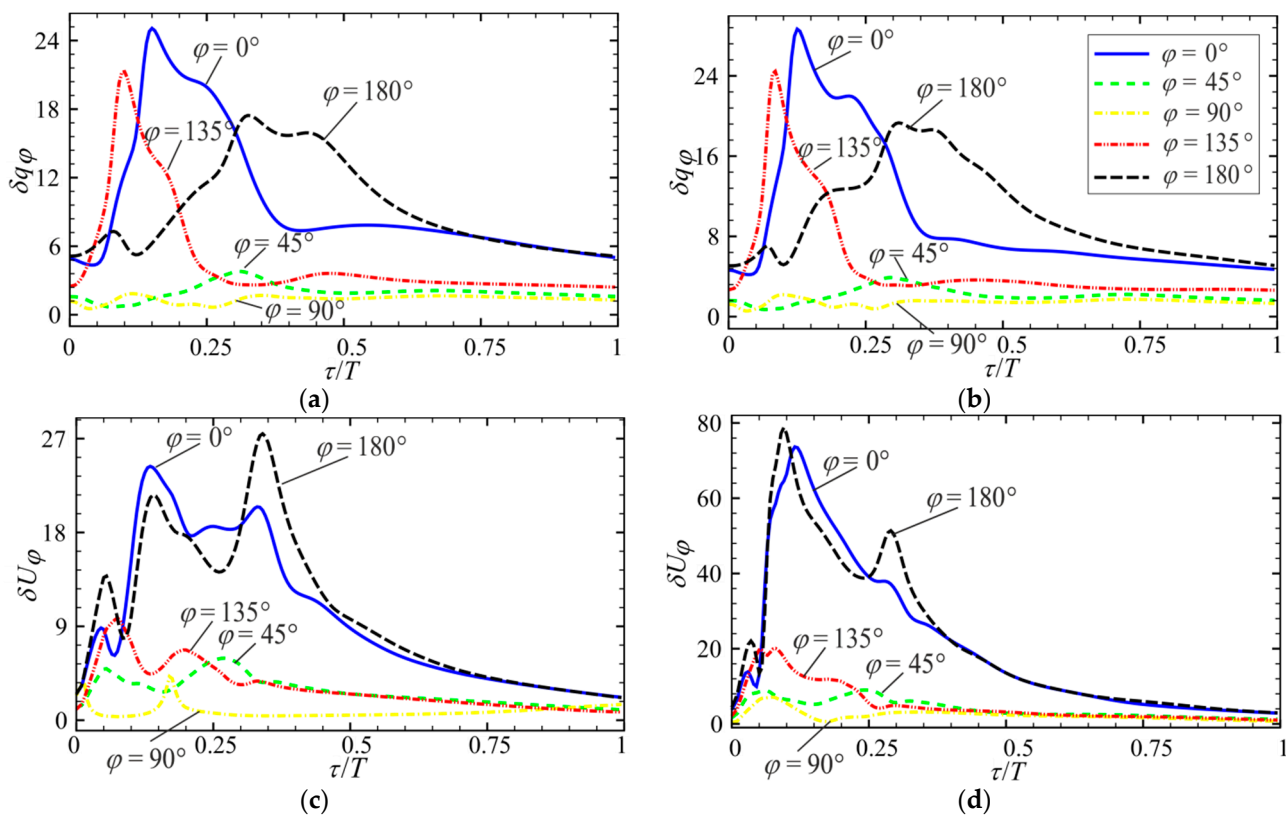


Figure 13. The effect of pulsations on the instantaneous local heat flux and velocity at $f = 0.5$ Hz for one period of pulsation. (a) Variation of heat flux ratio $\delta q_\varphi = q_{\varphi,p}/q_{\varphi,st}$ with τ/T at $A/D = 1.25$. (b) Variation of δq_φ with τ/T at $A/D = 4.5$. (c) Variation of velocity ratio $\delta U_\varphi = \langle U_{\varphi,p} \rangle / U_{\varphi,st}$ with τ/T at $A/D = 1.25$. (d) Variation of δU_φ with τ/T at $A/D = 4.5$.

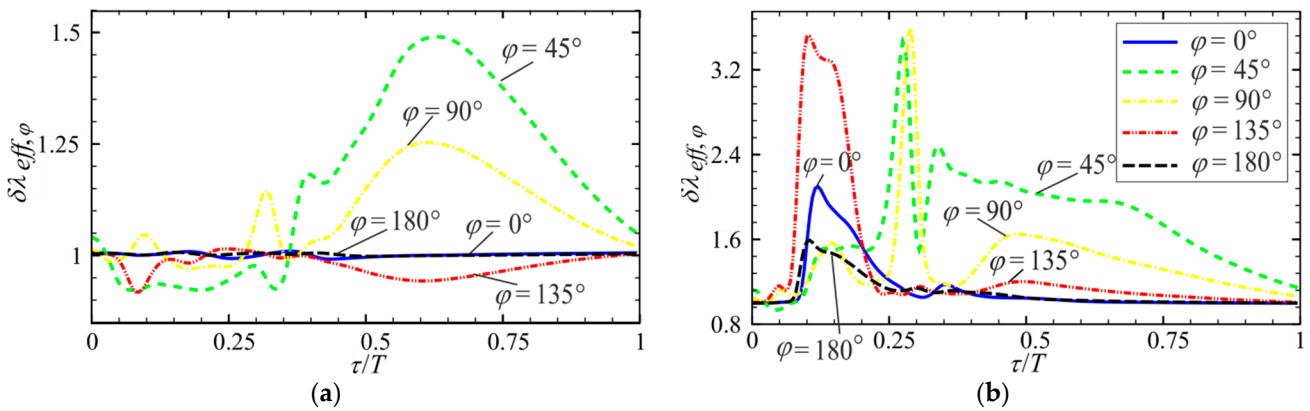


Figure 14. Cont.

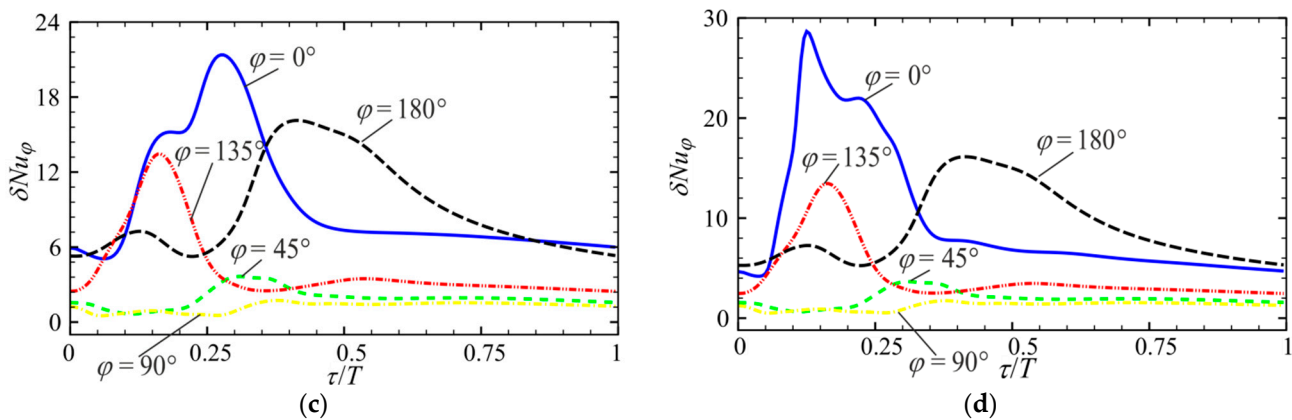


Figure 14. The effect of pulsations on the instantaneous local heat flux and velocity at $f = 0.5$ Hz for one period of pulsation. **(a)** Variation of effective thermal conductivity ratio $\delta\lambda_{eff,\varphi} = \lambda_{eff,\varphi,p}/\lambda_{eff,\varphi,st}$ with τ/T at $A/D = 1.25$. **(b)** Variation of $\delta\lambda_{eff,\varphi}$ with τ/T at $A/D = 4.5$. **(c)** Variation of the Nusselt number ratio $\delta Nu_\varphi = Nu_{\varphi,p}/Nu_{\varphi,st}$ with τ/T at $A/D = 1.25$. **(d)** Variation of δNu_φ with τ/T at $A/D = 4.5$.

3.3. Contour Plots of Temperature, Effective Thermal Conductivity, and Plots of the Velocity Vector

Figures 15–17 show the instantaneous temperature contour plots, effective thermal conductivity, and velocity vectors for a steady flow. The plots are shown only for three central rows of the tube bundle. The temperature distribution and effective thermal conductivity were correlated with the velocity vectors. For example, the results showed that two symmetric vortices formed between the rows in the regions $\varphi = 135^\circ$ and 225° . An increase in the effective thermal conductivity was also observed in this region. At the front and back of the tubes, the flow velocity was close to zero, and the flow temperature was the maximum, which was associated with poor flow circulation. Between the tubes ($\varphi = 90^\circ$), the flow velocity was the maximum and the temperature was the minimum.

Figures 18–20 show the fields of temperatures, the effective thermal conductivity, and velocity vectors at different phases of pulsations for the three central rows of the tube bundle. At almost all phases of pulsations, two symmetrical vortices formed in the wake of the tubes. The magnitude and size of the vortices increased with increasing input velocity. For phase (e), the size of the vortices between the rows was the maximum; the formation of two additional smaller vortices in the region ($\varphi = 0^\circ, 180^\circ$) was also noticeable. The flow rate was the maximum between the tubes ($\varphi = 90^\circ$) for phase (c). The increase in heat transfer was mainly associated with the increased vortex size between the rows. The maximum heat transfer enhancement occurred in areas ($\varphi = 0^\circ, 180^\circ$) (Figure 12). Molochnikov et al. [24] analyzed the flow structure and heat transfer in tube bundles at symmetric flow pulsations and reported the maximum heat transfer enhancement during the formation of two symmetric vortices in the wake of the cylinder in the tube bundle, which is consistent with this work. The temperatures and effective thermal conductivity correlated with the flow distribution in a pulsating flow. For example, for phase (e), the maximum effective thermal conductivity was observed in the regions of vortex formation. The maximum effective thermal conductivity value was observed for phase (g).

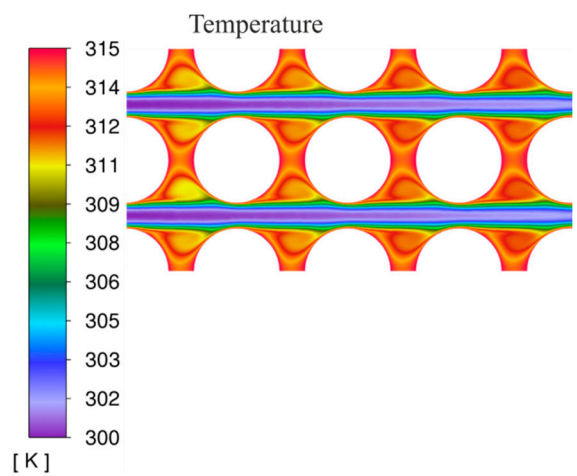


Figure 15. The temperature contour plots for the three central rows of the tube bundle at a steady flow.

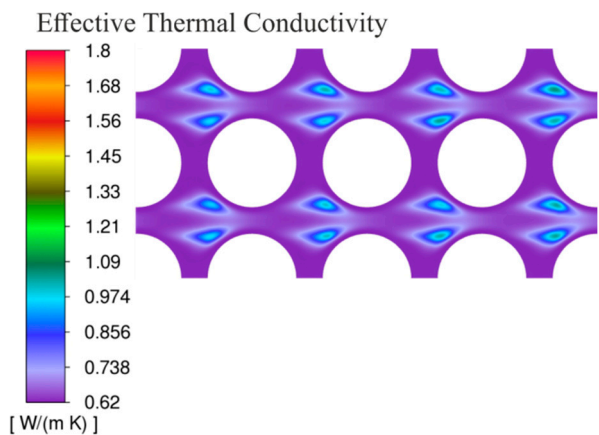


Figure 16. The effective thermal conductivity contour plots for the three central rows of the tube bundle at a steady flow.

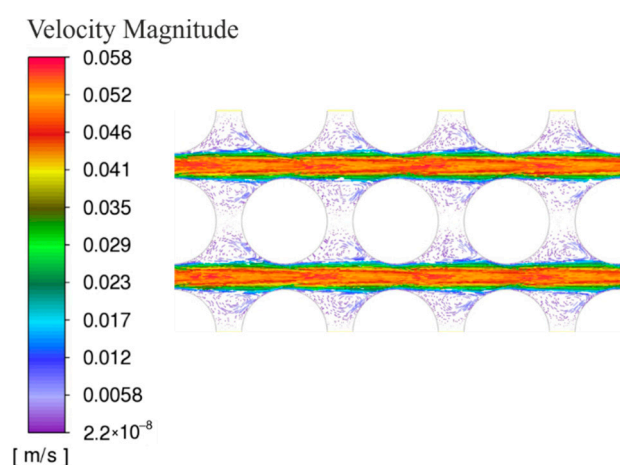


Figure 17. The velocity vector plots for the three central rows of the tube bundle at a steady flow.

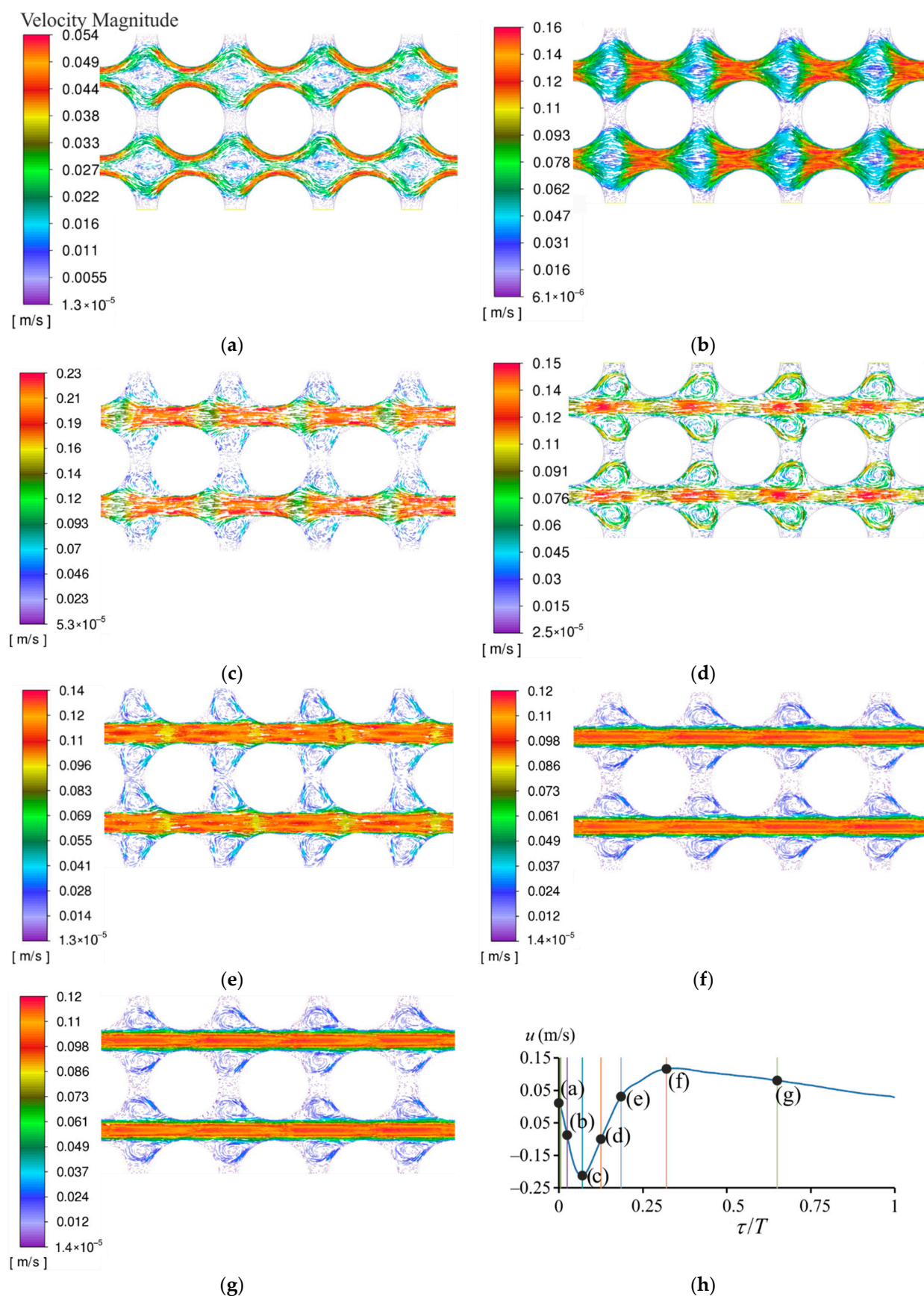


Figure 18. The instantaneous vector plots at different phases of pulsations for the three central rows of the tube bundle at $A/D = 3, f = 0.5$ Hz: (a) $\tau/T = 0.005$ (b) $\tau/T = 0.025$; (c) $\tau/T = 0.07$; (d) $\tau/T = 0.125$; (e) $\tau/T = 0.185$; (f) $\tau/T = 0.32$; (g) $\tau/T = 0.65$. (h) The velocity at tube bundle inlet for one period of pulsations and seven phase definition.

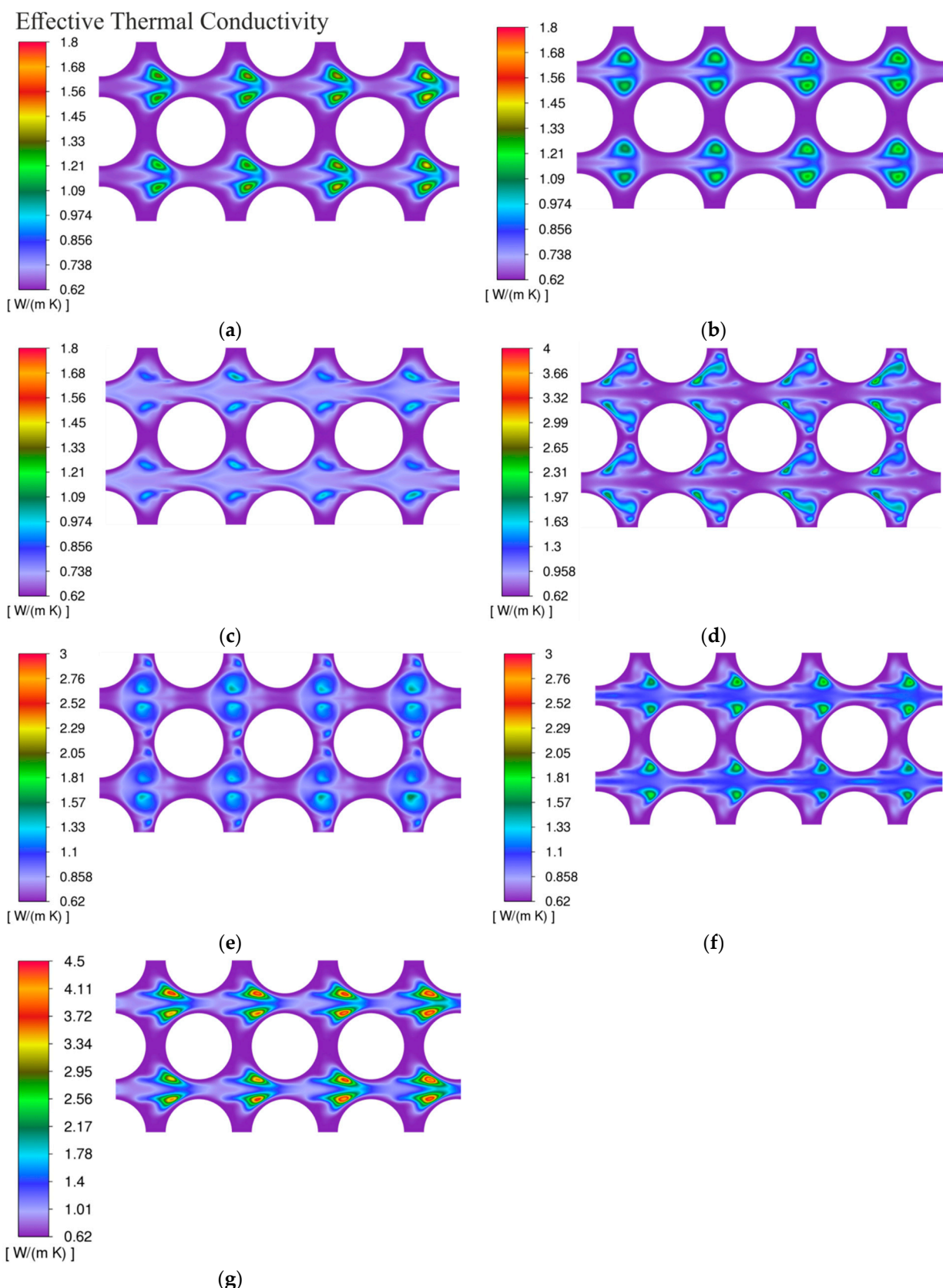


Figure 19. The instantaneous effective thermal conductivity contour plots at different phases of pulsations for the three central rows of the tube bundle at $A/D = 3$, $f = 0.5$ Hz: (a) $\tau/T = 0.005$; (b) $\tau/T = 0.025$; (c) $\tau/T = 0.07$; (d) $\tau/T = 0.125$; (e) $\tau/T = 0.185$; (f) $\tau/T = 0.32$; (g) $\tau/T = 0.65$.

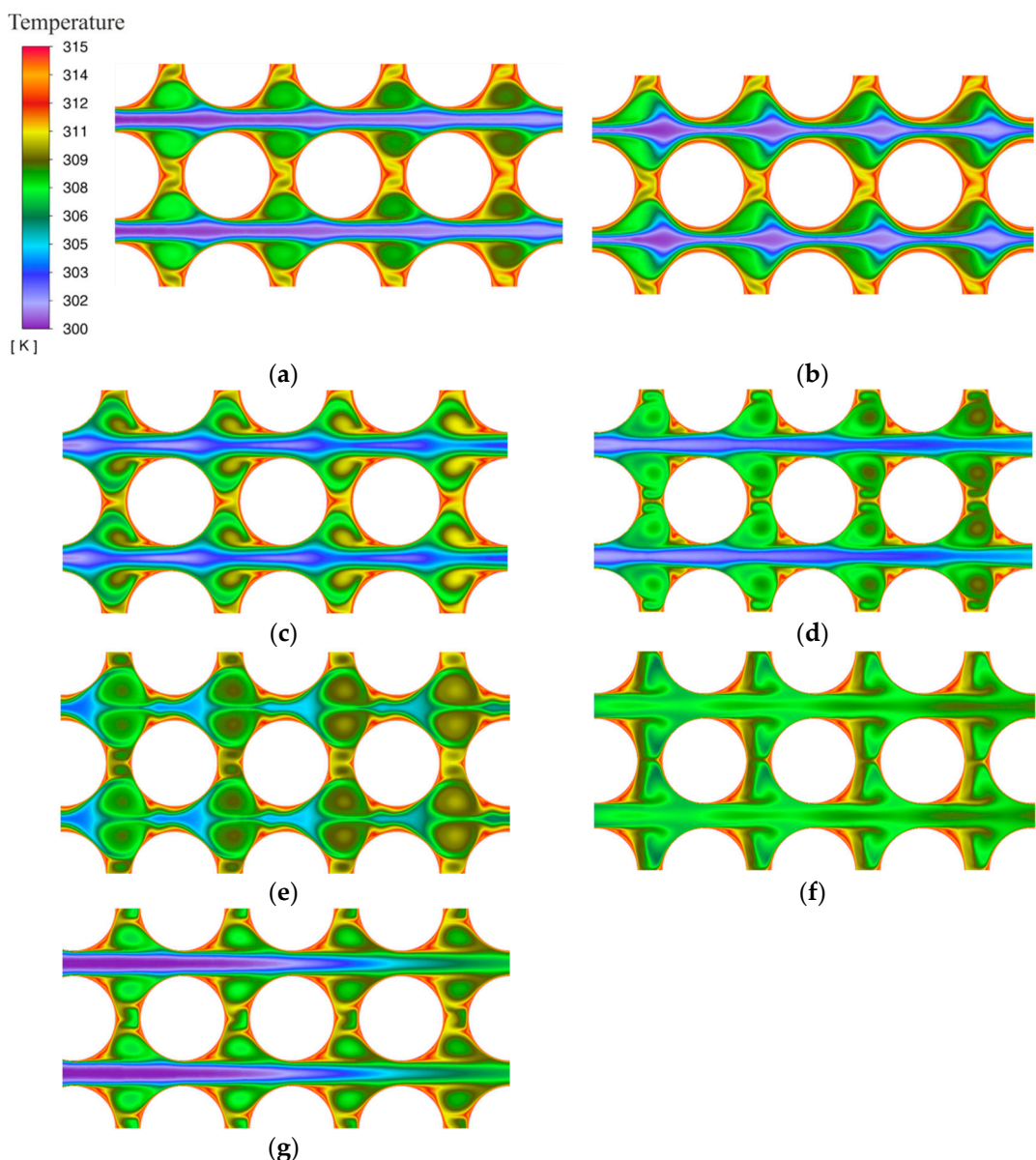


Figure 20. The instantaneous temperature contour plots at different phases of pulsations for the three central rows of the tube bundle at $A/D = 3, f = 0.5$ Hz: (a) $\tau/T = 0.005$ (b) $\tau/T = 0.025$; (c) $\tau/T = 0.07$; (d) $\tau/T = 0.125$; (e) $\tau/T = 0.185$; (f) $\tau/T = 0.32$; (g) $\tau/T = 0.65$.

4. Conclusions

In this work, the effect of asymmetric pulsating flows on the dynamics of the heat transfer and flow characteristics around the central cylinder in an in-line tube bundle was considered. An increase in the frequency and the amplitude of pulsations leads to a heat transfer enhancement. The heat transfer enhancement in a pulsating flow is mainly associated with an increase in the local flow velocity. With an increase in the frequency and amplitude of pulsations, an increase in the flow velocity occurs. The increased flow velocity leads to an increase in the size of the vortices between the rows of the tube bundle and the formation of two additional smaller vortices. An increase in the size and velocity of the vortices between the rows of the tube bundle is responsible for the heat transfer enhancement. The maximum velocity augmentation was observed in the front ($\varphi = 0^\circ$) and back of the cylinder ($\varphi = 180^\circ$), consistent with heat transfer augmentation in these areas. The maximum effective thermal conductivity augmentation was observed at $\varphi = 45^\circ$. The effective thermal conductivity increased with the increase in the pulsation amplitude.

Still, it practically did not change with the increase in pulsation frequency, although the heat transfer augmentation was always associated with higher frequency. Therefore, it follows that the effective thermal conductivity does not significantly affect the heat transfer enhancement. The maximum increase in heat transfer during the pulsations occurs when the flow velocity has the maximum acceleration.

Further studies will be aimed at studying the mechanisms of the heat transfer enhancement during pulsating flows in tube bundles with tube bundle configurations different to this work and a Reynolds numbers $Re > 1000$.

Author Contributions: Conceptualization, A.H. and A.K.; Methodology, V.B., L.K., D.B. and V.I.; Software, A.K.; Validation, V.B. and L.K.; Investigation, A.H., V.B. and L.K.; Formal analysis, V.B., L.K., D.B. and V.I.; Writing—original draft preparation, A.H. and A.K.; Writing—review and editing, A.H., D.B. and V.I.; Visualization, A.K. and D.B.; Supervision, A.H.; Project administration, A.H. All authors have read and agreed to the published version of the manuscript.

Funding: This research was funded by the Russian Science Foundation, grant number 18-79-10136, <https://www.rscf.ru/en/project/18-79-10136/>.

Institutional Review Board Statement: Not applicable.

Informed Consent Statement: Not applicable.

Data Availability Statement: The data presented in this study are available on request from the corresponding author.

Conflicts of Interest: The authors declare no conflict of interest.

Abbreviations

A	Dimensional amplitude of pulsation, m
A/D	Dimensionless relative amplitude of pulsation
D	Diameter of the tubes in tube bundle, m
D_j	Diameter of the hydraulic model elements, m
f	Frequency of pulsation, Hz
$F(\varphi, r)$	Area of the sector around the cylinder in the tube bundle, m^2
g	Gravity acceleration, m s^{-2}
H	Pressure in the hydraulic model elements, mH_2O
H_h	Pressure on the surface of the liquid in the hydraulic accumulator, mH_2O
$H_{p.c.}$	Pressure on the surface of the liquid in the pulsation chamber, mH_2O
k	Hydraulic resistance coefficient of the hydraulic model elements
l	Length of the hydraulic model elements, m
Nu	Nusselt number
P	Pressure, Pa
q	Heat flux, W m^{-2}
Q	Volumetric flow rate in the hydraulic model elements, $\text{m}^3 \text{s}^{-1}$
Re	Reynolds numbers
r_{min}/D	Minimum cell size in the near-wall region
S	Area of the hydraulic model elements, m^2
s/D	Relative transverse and longitudinal pitch of tube bundle
S_{h0}	Hole area at the bottom of the hydraulic accumulator, m^2
$S_{p.c.0}$	Hole area at the bottom of the pulsation chamber, m^2
St	Strouhal number
t_f	Flow temperature at the inlet of the tube bundle, $^\circ\text{C}$
t_s	Temperature around central cylinder in the fifth row of the tube bundle, $^\circ\text{C}$
t_w	Tube bundle wall temperature, $^\circ\text{C}$
u	Flow velocity at inlet of the tube bundle, m s^{-1}
U	Velocity around central cylinder in the fifth row of the tube bundle, m s^{-1}
$U_{x,y}$	Velocity components, m s^{-1}

y_{max}/D	Maximum mesh size related to the tube diameter
z_1	Liquid level in the hydraulic accumulator, m
z_2	Liquid level in the pulsation chamber, m
T	Period of the pulsation, s
T_1	First half-period of the pulsation, s
T_2	Second half-period of the pulsation, s
x	x-coordinate
y	y-coordinate
Greek symbols	
η	Kinematic viscosity, $m^2 \text{ s}^{-1}$
λ	Thermal conductivity, $\text{W m}^{-1} \text{ K}^{-1}$
λ_{eff}	Effective thermal conductivity, $\text{W m}^{-1} \text{ K}^{-1}$
λ_{turb}	Turbulent thermal conductivity, $\text{W m}^{-1} \text{ K}^{-1}$
τ	Time, s
τ_1	Start time of the pulsation period, s
τ_2	End time of the pulsation period, s
Δt	Temperature difference, $^{\circ}\text{C}$
Subscripts	
st	Steady flow
p	Pulsating flow
o	Averaged value over the surface of the cylinder wall in the tube bundle
a	Averaged value over the annular area around the cylinder in the tube bundle
φ	Averaged value depending on the azimuth angle
δ	Enhancement factor
Notations	
$\langle \rangle$	Averaged value over one period of the pulsation

References

- Bergles, A.E.; Manglik, R.M. Current progress and new developments in enhanced heat and mass transfer. *J. Enhanc. Heat Transf.* **2013**, *20*, 1–15. [[CrossRef](#)]
- Alam, T.; Kim, M.-H. A comprehensive review on single phase heat transfer enhancement techniques in heat exchanger applications. *Renew. Sustain. Energy Rev.* **2018**, *81*, 813–839. [[CrossRef](#)]
- Wang, W.; Shuai, Y.; Li, B.; Li, B.; Lee, K.-S. Enhanced heat transfer performance for multi-tube heat exchangers with various tube arrangements. *Int. J. Heat Mass Transf.* **2021**, *168*, 120905. [[CrossRef](#)]
- Nguyen, D.H.; Ahn, H.S. A comprehensive review on micro/nanoscale surface modification techniques for heat transfer enhancement in heat exchanger. *Int. J. Heat Mass Transf.* **2021**, *178*, 121601. [[CrossRef](#)]
- Maradiya, C.; Vadher, J.; Agarwal, R. The heat transfer enhancement techniques and their Thermal Performance Factor. *Beni-Suef Univ. J. Basic Appl. Sci.* **2018**, *7*, 1–21. [[CrossRef](#)]
- Li, X.; Zhu, D.; Sun, J.; Mo, X.; Liu, S. Heat transfer and pressure drop for twisted oval tube bundles with staggered layout in crossflow of air. *Appl. Therm. Eng.* **2019**, *148*, 1092–1098. [[CrossRef](#)]
- Khalatov, A.A.; Kovalenko, G.V.; Meiris, A.Z. Heat Transfer in Air Flow Across a Single-Row Bundle of Tubes With Spiral Grooves. *J. Eng. Phys. Thermophys.* **2018**, *91*, 64–71. [[CrossRef](#)]
- Pongsoi, P.; Pikulkajorn, S.; Wongwises, S. Effect of fin pitches on the optimum heat transfer performance of crimped spiral fin-and-tube heat exchangers. *Int. J. Heat Mass Transf.* **2012**, *55*, 6555–6566. [[CrossRef](#)]
- Mavridou, S.G.; Konstandinidis, E.; Bouris, D.G. Experimental evaluation of pairs of inline tubes of different size as components for heat exchanger tube bundles. *Int. J. Heat Mass Transf.* **2015**, *90*, 280–290. [[CrossRef](#)]
- Wangnipparnto, S.; Tiansuwan, J.; Kiatsiriroat, T.; Wang, C.C. Performance analysis of thermosyphon heat exchanger under electric field. *Energy Convers. Manag.* **2003**, *44*, 1163–1175. [[CrossRef](#)]
- Cheng, L.; Luan, T.; Du, W.; Xu, M. Heat transfer enhancement by flow-induced vibration in heat exchangers. *Int. J. Heat Mass Transf.* **2009**, *52*, 1053–1057. [[CrossRef](#)]
- Jeng, T.-M.; Tzeng, S.-C.; Xu, R. Heat transfer characteristics of a rotating cylinder with a lateral air impinging jet. *Int. J. Heat Mass Transf.* **2014**, *70*, 235–249. [[CrossRef](#)]
- Cheng, P.; Zhao, T.S. Heat transfer in oscillatory flows. *Annu. Rev. Heat Transf.* **1998**, *9*, 359–420. [[CrossRef](#)]
- Herman, C. The impact of flow oscillations on convective heat transfer. *Annu. Rev. Heat Transf.* **2000**, *11*, 495–561. [[CrossRef](#)]
- Elshafei, E.A.M.; Safwat Mohamed, M.; Mansour, H.; Sakr, M. Experimental study of heat transfer in pulsating turbulent flow in a pipe. *Int. J. Heat Fluid Flow* **2008**, *29*, 1029–1038. [[CrossRef](#)]
- Olayiwola, B.; Walzel, P. Cross-flow transport and heat transfer enhancement in laminar pulsed flow. *Chem. Eng. Processing Process Intensif.* **2008**, *47*, 929–937. [[CrossRef](#)]

17. Kikuchi, Y.; Suzuki, H.; Kitagawa, M.; Ikeya, K.-I. Effect of Pulsating Strouhal Number on Heat Transfer around a Heated Cylinder in Pulsating Cross-Flow. *JSME Int. J. Ser. B* **2000**, *43*, 250–257. [[CrossRef](#)]
18. Fu, W.-S.; Tong, B.-H. Numerical investigation of heat transfer from a heated oscillating cylinder in a cross flow. *Int. J. Heat Mass Transf.* **2002**, *45*, 3033–3043. [[CrossRef](#)]
19. Zheng, Y.; Li, G.; Guo, W.; Dong, C. Lattice Boltzmann simulation to laminar pulsating flow past a circular cylinder with constant temperature. *Heat Mass Transf.* **2017**, *53*, 2975–2986. [[CrossRef](#)]
20. Ji, T.H.; Kim, S.Y.; Hyun, J.M. Experiments on heat transfer enhancement from a heated square cylinder in a pulsating channel flow. *Int. J. Heat Mass Transf.* **2008**, *51*, 1130–1138. [[CrossRef](#)]
21. Luo, X.; Zhang, W.; Dong, H.; Thakur, A.K.; Yang, B.; Zhao, W. Numerical analysis of heat transfer enhancement of fluid past an oscillating circular cylinder in laminar flow regime. *Prog. Nucl. Energy* **2021**, *139*, 103853. [[CrossRef](#)]
22. Mikheev, N.I.; Molochnikov, V.M.; Mikheev, A.N.; Dushina, O.A. Hydrodynamics and heat transfer of pulsating flow around a cylinder. *Int. J. Heat Mass Transf.* **2017**, *109*, 254–265. [[CrossRef](#)]
23. Molochnikov, V.M.; Mikheev, N.I.; Mikheev, A.N.; Paereliy, A.A. Heat transfer from a cylinder in pulsating cross-flow. *Thermophys. Aeromech.* **2017**, *24*, 569–575. [[CrossRef](#)]
24. Molochnikov, V.M.; Mikheev, A.N.; Aslaev, A.K.; Dushina, O.A.; Paereliy, A.A. Heat transfer of a tube bundle in a pulsating flow. *Thermophys. Aeromech.* **2019**, *26*, 547–559. [[CrossRef](#)]
25. Molochnikov, V.M.; Mikheev, A.N.; Aslaev, A.K.; Goltsman, A.E.; Paereliy, A.A. Flow structure between the tubes and heat transfer of a tube bundle in pulsating flow. *J. Phys. Conf. Ser.* **2018**, *1105*, 012024. [[CrossRef](#)]
26. Liang, C.L.; Papadakis, G. Study of the effect of flow pulsation on the flow field and heat transfer over an inline cylinder array using LES. *Eng. Turbul. Model. Exp.* **2005**, *6*, 813–822. [[CrossRef](#)]
27. Wu, Z.; You, S.; Zhang, H.; Zheng, W. Experimental investigation on heat transfer characteristics of staggered tube bundle heat exchanger immersed in oscillating flow. *Int. J. Heat Mass Transf.* **2020**, *148*, 119125. [[CrossRef](#)]
28. Chen, S.; Huang, Q.; Liang, M.; Chen, H.; Chen, L.; Hou, Y. Numerical study on the heat transfer characteristics of oscillating flow in cryogenic regenerators. *Cryogenics* **2018**, *96*, 99–107. [[CrossRef](#)]
29. Mulcahey, T.I.; Pathak, M.G.; Chiaasiaan, S.M. The effect of flow pulsation on drag and heat transfer in an array of heated square cylinders. *Int. J. Therm. Sci.* **2013**, *64*, 105–120. [[CrossRef](#)]
30. Balabani, S.; Yianneskis, M. An experimental study of the mean flow and turbulence structure of cross-flow over tube bundles. *Proc. Inst. Mech. Eng. Part C-J. Mech. Eng. Sci.* **1996**, *210*, 317–331. [[CrossRef](#)]
31. Shah, R.K.; Sekulić, D.P. *Fundamentals of Heat Exchanger Design*; John Wiley & Sons: Hoboken, NJ, USA, 2003.
32. Zhukauskas, A.A.; Ulinskas, R. *Heat Transfer in Banks of Tubes in Crossflow of fluid*; Mintis: Vilnius, Lithuania, 1968; p. 200. (In Russian)
33. Zukauskas, A. Heat Transfer from Tubes in Crossflow. *Adv. Heat Transf.* **1972**, *18*, 87–159.
34. Ye, Q.; Zhang, Y.; Wei, J. A comprehensive review of pulsating flow on heat transfer enhancement. *Appl. Therm. Eng.* **2021**, *196*, 117275. [[CrossRef](#)]
35. Sung, H.J.; Hwang, K.S.; Hyun, J.M. Experimental-study on mass-transfer from a circular-cylinder in pulsating flow. *Int. J. Heat Mass Transf.* **1994**, *37*, 2203–2210. [[CrossRef](#)]
36. Cheng, C.-H.; Hong, J.-L.; Aung, W. Numerical prediction of lock-on effect on convective heat transfer from a transversely oscillating circular cylinder. *Int. J. Heat Mass Transf.* **1997**, *40*, 1825–1834. [[CrossRef](#)]
37. Konstantinidis, E.; Balabani, S.; Yianneskis, M. Relationship Between Vortex Shedding Lock-On and Heat Transfer. *Chem. Eng. Res. Des.* **2003**, *81*, 695–699. [[CrossRef](#)]
38. Perwaiz, J.; Base, T.E. Heat-transfer from a cylinder and finned tube in a pulsating cross-flow. *Exp. Therm. Fluid Sci.* **1992**, *5*, 506–512. [[CrossRef](#)]
39. Ilyin, V.K.; Sabitov, L.S.; Hajbullina, A.I.; Hayrullin, A.R.; IOP. Factors influencing on the thermal flow with the cross-section of the corridor tube bundle in low-frequency non-symmetric pulsations. *IOP Conf. Ser. Mater. Sci. Eng.* **2017**, *240*, 012026. [[CrossRef](#)]
40. Abramov, A.G.; Levchenya, A.M.; Smirnov, E.M.; Smirnov, P.E. Numerical simulation of liquid metal turbulent heat transfer from an inline tube bundle in cross-flow. *St. Petersburg Polytech. Univ. J. Phys. Math.* **2015**, *1*, 356–363. [[CrossRef](#)]
41. Ivanov, N.G.; Kirillov, A.I.; Smirnov, E.M.; Ris, V.V. Numerical Modeling of Buoyancy-Induced Fluid Flow and Heat Transfer in a Staggered Tube Bank. In Proceedings of the 2010 14th International Heat Transfer Conference, Washington, DC, USA, 8–13 August 2010; pp. 545–551.
42. Hajbullina, A.; Hajrullin, A.; Il'in, V. Heat transfer in the flow channel in tube bundle corridor type under imposed on the flow liquid of upstream low-frequency asymmetrical pulsations. *Power Eng. Res. Equip. Technol.* **2016**, *18*, 56–67. (In Russian) [[CrossRef](#)]
43. Larock, B.E.; Jeppson, R.W.; Watters, G.Z. *Hydraulics of Pipeline Systems*; CRC Press: Boca Raton, FL, USA, 2000.
44. Spalart, P.; Allmaras, S. A One-Equation Turbulence Model for Aerodynamic Flow. In Proceedings of the 30th Aerospace Sciences Meeting and Exhibit, Reno, NV, USA, 6–9 January 1992; p. 439.
45. Wang, Y.Q.; Jackson, P.L. Turbulence Modeling Applied to Flow Through a Staggered Tube Bundle. *J. Thermophys. Heat Transf.* **2010**, *24*, 534–543. [[CrossRef](#)]

46. Kim, S.-M.; Ghiaasiaan, S.M. Numerical Modeling of Laminar Pulsating Flow in Porous Media. *J. Fluids Eng.* **2009**, *131*, 041203. [[CrossRef](#)]
47. Haibullina, A.I. Improving the Efficiency of Heat Exchangers due to Low-Frequency Flow Pulsations. Ph.D. Thesis, Kazan State Power Engineering University, Kazan, Russia, 2017. (In Russian).